Numerical analysis of the tread grooves' acoustic resonances for the investigation of tyre noise

Luca Rapino[1]
Politecnico di Milano, Department of Mechanical Engineering
Via La Masa 1, 20156 Milano, Italy
luca.rapino@polimi.it

Francesco Ripamonti
Politecnico di Milano, Department of Mechanical Engineering
Via La Masa 1, 20156 Milano, Italy
francesco.ripamonti@polimi.it

Simone Baro
Pirelli Tyre S.p.A.
Viale Piero e Alberto Pirelli 25, 20126 Milano, Italy
simone.baro@pirelli.com

Roberto Corradi
Politecnico di Milano, Department of Mechanical Engineering
Via La Masa 1, 20156 Milano, Italy
roberto.corradi@polimi.it

ABSTRACT

Tyre/road noise is one of the major sources of noise pollution in urban areas. This phenomenon can be described as the combined effect of several generation and amplification mechanisms. Acoustic resonances due to the tread grooves at the footprint region, also known as pipe resonances, are particularly important since they can generate high noise levels if they combine with harmonic generation mechanisms. This paper deals with a numerical investigation of this phenomenon and describes modelling approaches that might be used to estimate the frequencies and the mode shapes of these resonances.

Keywords

Tyre/road noise; airborne exterior noise; amplification mechanism; pipe resonances; numerical models.

[1] Corresponding author.

1. INTRODUCTION

A considerable number of people are exposed to high levels of road traffic noise [1]. This problem is mainly due to the tyre/road interaction, which is the dominant noise source for almost all types of driving conditions [2] and it is even more evident in the case of electric and hybrid powertrains. The most effective way to reduce tyre/road noise is the development of low-noise tyres. However, this task is challenging due to the complexity of the phenomena involved.

Tyre/road noise is caused by several generation and amplification mechanisms [3–7], which are strictly related to tyre design parameters. In particular, the tread pattern plays a crucial role [8–10], since it is both a generator, due to the tread impact and the air pumping mechanisms [11,12], and an amplifier, due to the acoustic resonances of the air volumes inside the grooves at the footprint region. These mechanisms are important since the vibroacoustic dynamic of the footprint region dominates the overall noise [13,14] because of horn amplification [15–17]. To reduce the tyre/road noise, it is therefore fundamental to avoid the combination of the grooves' acoustic resonances and the generation mechanisms. For this reason, investigating and modelling these resonances are relevant for the tyre industry.

The air volume inside a groove can be modelled as a duct of length L, in which air displacements may generate standing waves. Basic analytical models show that, depending on the boundary conditions of the two ends, the first resonance frequency is $f = \frac{c}{2L}$ (both ends closed or open) or $f = \frac{c}{4L}$ (one end closed and the other open), where c is the sound speed. However, the actual resonance frequency is typically lower since,

for open ends, the acoustic wavelength is longer than the geometrical length of the groove. This aspect can be included by using complex impedance models, or by considering an additional duct length ΔL for each open end [18,19]. The latter, also known as the "end correction" approach, is discussed in [3,20] for tyre/road noise applications, and expressions for evaluating ΔL provided the grooves' cross-sections are reported. Instead, in [21] the author suggests an end correction in the range of $\Delta L = 15 - 20$ mm.

Nonetheless, this simplified analytical approach cannot describe the acoustic resonances of real tread patterns, which are made up of several interconnected grooves. To investigate such systems, a numerical approach is required. For this reason, in [22,23] the authors used the Boundary Element Method (BEM) and the Finite Element Method (FEM) to model a network of ducts in a horn-like structure, with the intent of studying the acoustic amplifications of this system and tuning the resonance frequencies. Another study that involves numerical FEM models of the grooves' acoustic resonances can be found in [24]

This paper deals with FEM models for the analysis of the tread grooves' acoustic resonances. First, the outcomes of a parametric analysis based on simple geometries are shown, with the aim of describing some fundamental aspects of the phenomenon. Then, the discussion focuses on three approaches that might be employed during tyre design. Therefore, a realistic tread pattern geometry is used, and comparisons are performed. It is worth mentioning that in this paper the analysis of the acoustic resonances aims to evaluate their frequencies and mode shapes only, whereas a comprehensive model that

simulates the sound field of a rolling tyre is out of the scope of this work. Instead, this topic is discussed in other references [7,14,25].

This paper is organised as follows. In Section 2, a general overview of the methodology and possible modelling approaches are presented. Then, fundamental concepts of tread grooves' acoustic resonances are discussed through interpretative models of a circumferential groove with lateral grooves. In Section 3, the modelling approaches are used to analyse the acoustic resonances of a tread pattern. In addition, a modelling approach based on a network of mono-dimensional finite elements is presented, with the intent of describing an alternative approach to study the grooves' resonances. The limitations and strengths of the approaches are also discussed. Finally, the conclusions of this work are drawn in the last section.

2. METHODOLOGY AND FUNDAMENTALS OF THE TREAD GROOVES' ACOUSTIC RESONANCES

In this work, the grooves' acoustic resonances were investigated using acoustic Finite Element models. According to this approach, the geometry of interest is discretised into finite elements and the mass and stiffness matrices of the system, M and K, are assembled [26]. Then, the acoustic resonances can be found by solving the eigenvalue problem of an undamped system:

$$(-\omega_n^2 M + K)\ \varphi_{\mathrm{n}} = 0 \qquad (1)$$

where the unknowns are the natural frequencies $f_n = \omega_n/2\pi$ and the mode shapes φ_n.

Different approaches can be used when defining these models. Firstly, simulations may differ in terms of modelled air volume. In some cases, only the air inside the tread grooves at the footprint region is included, whereas other simulations can be based on a larger volume that also includes the air around the whole tyre. In addition, for simulations based only on the air inside the tread grooves, the so-called “end corrections” might also be included to improve the results. On the other hand, the methodology for describing the geometries (i.e. tread grooves and tyre surfaces) can be based on CAD (Computer-Aided Design) models, on simplified approaches, or on the results of numerical structural simulations, where a deformed tyre geometry is considered. In this paper, several approaches are discussed and compared. Therefore, for the sake of clarity, their names and main features are listed in Table 1. For Approaches 1 and 2, models were defined within the Wave6 commercial software, whereas Approaches 3a and 3b are based on codes implemented within Matlab by the authors.

Before comparing the modelling approaches, in this section the fundamental principles of the tread grooves’ acoustic resonances are introduced and simple interpretative models are used to investigate how lateral grooves influence the acoustic resonances of a circumferential groove. “Approach 1” is used, since only the grooves’ air volumes are modelled. Therefore, the effect of the air surrounding the footprint region is neglected and no end correction is applied.

First of all, a model of a circumferential groove was defined, considering a rectangular cross-section of 10 mm x 7 mm and a footprint length of 140 mm. These dimensions were

122 based on the tread pattern geometry considered later in this work. A pressure release
123 boundary condition was applied to the grooves' terminations and no end correction was
124 considered. By solving the eigenvalue problem associated with the model (refer to Eq. 1),
125 two acoustic modes were found within the frequency range of interest 0-3 kHz. This range
126 was chosen given that tyre noise occurs mainly at these frequencies. The model's
127 geometry and the results are shown in Figure 1.
128
129 The resulting modes agree with the analytical formulation, both in terms of natural
130 frequencies and mode shapes. In particular, the first resonance shows two nodes at the
131 groove's ends and an antinode at the centre, whereas the second resonance shows two
132 antinodes. It is worth pointing out that, for tyre noise applications, within the frequency
133 range of interest the acoustic modes are characterised by plane waves only. Indeed,
134 considering a duct with an equivalent circular cross-section, the cut-on frequency of
135 cross-sectional modes is:

$$f_{cut-on} = 1.841 \cdot \frac{c}{\pi d} \tag{2}$$

136 where c stands for the sound speed and d for the duct diameter. Taking into account that
137 most of the tyre noise is concentrated below 3 kHz, grooves with diameters larger than
138 65 mm would be required to develop cross-sectional modes. Since this dimension is
139 typically much smaller, it is safe to assume that cross-sectional modes are not relevant to
140 this application.
141

Then, a set of lateral grooves was included in the model, considering a cross-section area of 10 mm x 3 mm and a length of 20 mm. Grooves were positioned with a spacing of 25 mm to schematise an ideal tyre with a tread pattern made up of 80 pitches distributed along a circumference of 2 m. All lateral groove terminations were assumed to end in open air. As a consequence, a pressure release boundary condition was applied. The model and the results are represented in Figure 2.

It can be observed that the inclusion of the lateral grooves caused no significant variation of the mode shapes along the circumferential groove. In addition, the pressure field inside a lateral groove can be described as a transition from a null pressure (imposed at the open ends) to the pressure at the intersection with the circumferential groove. This is valid up to the frequency range of the lateral grooves' resonances, which is typically higher than that of the circumferential grooves' resonances. This range can be estimated considering that the resonance of an open-ended lateral groove of length L_{lat} is approximately at $f = c/(2L_{lat})$. For this model, it was confirmed that these resonances are present from approximately 8 kHz.

The results show higher natural frequencies than the model of a circumferential groove only. This behaviour can be explained considering that, even though a progressive transition is present, the null pressure at the lateral groove ends is a constraint for the circumferential groove's air volume, generating a stiffening effect. This effect has a higher impact on the first resonance (+53% frequency shift) than the second one (+12% shift).

A closed-end boundary condition was also imposed at the lateral grooves' terminations and the results are represented in Figure 3. In this case, when the circumferential groove resonates, the lateral grooves' air volumes vibrate accordingly, without a transition to a null pressure. This causes an increment in the modal mass of the system, without introducing an additional stiffening effect. Therefore, comparing the results against those for the circumferential groove model, a reduction of the natural frequencies is obtained. In this condition, the lateral grooves behave as quarter-wave resonators and may resonate at much lower frequencies than the open-end lateral grooves. In this case, a qualitative estimate can be obtained considering that these resonances are present even below $f = c/(4L_{lat})$. For this model, these resonances are visible starting from 3kHz.

To extend the analysis, additional simulations were performed to investigate the effect of the lateral grooves' length. The results are shown in Figure 4, considering both open-end lateral grooves (on the left) and a closed-end boundary condition (on the right). Each plot represents the trend of the first (in black) and second resonance frequencies (in red) for the variation of the lateral groove length. Attention should be paid to the two y-scales included in the representations, one for each resonance frequency. The results show that, for both boundary conditions, longer lateral grooves cause lower resonance frequencies. For the open-end boundary condition, this can be explained considering that a lower stiffening effect is present if the null pressure condition is imposed at a higher distance from the circumferential grooves. On the other hand, for the closed-ends case, a greater lateral groove length causes an increment in air volumes, and thus a higher modal mass.

Finally, comparing the two black curves in Figure 4, it can be stated that longer lateral grooves determine higher reductions in the first resonance frequency in the case of open-ends.

For these analyses, a 25 mm spacing between lateral grooves was considered, resulting in six grooves connected to the circumferential one. Even though this length was chosen as representative of a car tyre, an analysis of the influence of the number of lateral grooves at the footprint region was performed. In Figure 5, the effect on the resonance frequencies of a transition from zero to six 20 mm lateral grooves is shown. The stiffening effect is confirmed for the open-end lateral grooves as well as the mass effect for closed-end ones. In conclusion, the higher the number of lateral grooves, the higher the influence of these two mechanisms.

During tyre rolling, the tread pattern enters the contact patch at the inlet region and moves towards the outlet, causing a progressive displacement of the grooves along the circumferential direction. For acoustic analyses, this can be simplified by assuming that the circumferential grooves' geometry is not affected, whereas a progressive shift of the lateral grooves along the circumferential direction is present. Therefore, an analysis of the variation of the resonance frequencies due to the position of the lateral grooves was performed. This analysis was parametrised by expressing the lateral grooves' displacement as a fraction of one pitch distance (i.e. the spacing between the lateral grooves). In fact, for mono-pitched patterns such as the one considered in this section,

the configuration of the lateral grooves is periodic in relation to the pitch distance. The outcomes of the investigation are shown in Figure 6 for both open-end and closed-end boundary conditions. Paying attention to the ranges of the y-axes, it can be concluded that the variations of the resonance frequencies are very limited and negligible compared to the other effects discussed previously. However, this conclusion is significant, since it justifies the choice of studying the acoustic resonances using a static geometry and neglecting the motion of the tread pattern at the footprint region.

3. MODELLING APPROACHES FOR ANALYSING THE ACOUSTIC RESONANCES OF A TREAD PATTERN

The aim of this section is to discuss different modelling approaches for the analysis of the acoustic resonances of a tread pattern geometry. Reference is made to the classification introduced in Table 1. To define a case study, it was observed that most summer tyres are made with four circumferential grooves and five tread block sections, the so-called “ribs”. At the central ribs, circumferential grooves are connected through narrow lateral grooves called “sipes”, whereas the outer ribs are characterised by open-ended lateral grooves. Based on this layout, the geometry of a simplified tread pattern was defined. A 225/55R17 tyre size with a known footprint length and width was considered.

3.1 Approach 1 and Approach 2

First of all, the grooves' air volumes at the footprint region were modelled according to Approach 1, considering open-end boundary conditions at the outer terminations of the grooves. The resulting model is represented in Figure 7. It can be noticed that, to simplify the definition of the geometrical model, this investigation was performed using a rectangular footprint.

Once the model setup was completed, the natural frequencies and the mode shapes were evaluated by solving the eigenvalue problem. The resulting modes were classified according to a (n, m) nomenclature, where n stands for the number of the antinodes along the circumferential direction and m for the mode number considering the antinodes along the lateral direction. In Figure 8, the modes with the lowest frequencies, representative of the whole family $(1, m)$, are shown. These modes are dominated according to the pressure variations at the circumferential grooves that, depending on the resonance considered, may resonate in-phase or out-of-phase with one another. This behaviour is due to the presence of the sipes, which couple the dynamic response of the circumferential grooves, causing a mutual influence. Due to this trend, the pressure fields inside the sipes may be characterised by progressive pressure transitions, as shown in detail in Figure 8. It is worth pointing out that, in real conditions, a cross-talk effect between circumferential grooves is also present due to the air volume that surrounds the footprint region. However, this effect is not included in this modelling approach. The results also show that the higher the variations along the lateral direction (i.e. the higher

the mode number m), the higher the natural frequency associated with the mode. This trend is justified by the acoustic wave equation:

$$-\omega^2\bar{p} = \mathrm{c}^2 \cdot \nabla^2\bar{p} \qquad \text{with } p(\boldsymbol{x},t) = \bar{p}(\boldsymbol{x}) \cdot e^{j\omega t} \tag{3}$$

which states that, the higher the pressure gradient, the higher the frequency. To complete the discussion, it can be noticed that the lateral grooves show no particular dynamics in the frequency range of interest, except for providing a smooth transition from the pressure field inside the footprint region to the null pressure at the footprint boundary.

Even though Approach 1 is useful for interpreting the trends of acoustic resonances, it is not suitable for quantitative evaluations. This limitation is due to the simplified boundary conditions that neglect the dynamics of the air outside the footprint region. In particular, imposing a null pressure as an open-end boundary condition leads to an overestimation of the natural frequencies.

To avoid this issue, an acoustic model based on Approach 2 was defined. To be consistent with the previous analysis, the envelope of a deformed 225/55R17 tyre equipped with the same tread pattern was used. The deformed tyre geometry was extracted from the results of a structural simulation, considering a vertical load of 500 kg and the tyre pressed on a drum with a diameter of 2.5 m. It is worth mentioning that the resulting geometry and the simplified model share the same footprint length and width. In Figure 9, the tyre and the ground surfaces are represented. It can be noticed that the surface in contact with the ground is not present, as the air volume is delimited only by the grooves and the

tyre surface that is not in contact with the ground. To complete the model, an air volume that surrounds the whole tyre and the drum was defined.

Then, the acoustic resonances were evaluated by solving the eigenvalue problem associated with the model. In this case, several additional acoustic resonances related to the air volume around the tyre were present. However, among these additional results, it was possible to identify the tread grooves' acoustic resonances due to their peculiar mode shapes, characterised by localised high-pressure amplitudes in the footprint region. Referring to the modes' nomenclature introduced previously, the results of the mode family $(1, m)$ are shown in Figure 10 as pressure maps evaluated at the tyre's outer surface (in the region highlighted in dark grey in Figure 9).

The results show that the main characteristics of the pressure fields and the sequence of the mode shapes agree with the outcomes of Approach 1. However, focusing on the details of each pressure field, it can be noticed that Approach 2 estimates a non-null pressure at the circumferential grooves' ends. In fact, in this case, the null pressure is present outside the footprint region, obtaining an acoustic wavelength longer than the geometrical length of the grooves. As a consequence, comparing the resonance frequencies against those for Approach 1, a significant reduction is present. The comparison also shows that the shift associated with each frequency is not constant, and modes at lower frequencies are influenced more (e.g. the frequency shift of the first mode is -602.4 Hz, whereas the second mode has a shift of -452.5 Hz). For the sake of

conciseness and clarity, the natural frequencies evaluated using all the modelling approaches discussed in this paper are reported in Table 2.

Even though Approach 2 is recommended for quantitative predictions due to the more physical description of the boundary conditions, it involves a higher level of complexity than Approach 1. In particular, more effort is required for defining a deformed treaded tyre geometry, as a structural simulation is needed to model the deformed tyre. This aspect limits the possibility of performing rapid changes to the tread pattern design and assessing the trends of the acoustic resonances. In addition, the acoustic model for Approach 2 is based on larger air volumes, causing higher computation times due to the higher number of degrees of freedom to be solved. In conclusion, taking into account the model setup and the computational efforts, Approach 2 does not exclude simplified approaches such as Approach 1, and should be considered as a complementary tool for the analysis of acoustic resonances.

3.2 Approach 3a and Approach 3b

The results of Approach 1 suggest that the pressure field at the footprint region changes only along the grooves' axial directions. For this reason, to define simpler and faster models, an alternative approach based on mono-dimensional finite elements is described here.

A mono-dimensional (1D) acoustic finite element consists of a segment of length L that models the pressure field inside a duct of cross-section A, assuming that the pressure can

change only along the duct's axial direction x. Below the cut-on frequency of cross-sectional modes, duct acoustic resonances can be modelled with these elements. In this work, this pressure field is approximated using a cubic polynomial function:

$$p(x) = ax^3 + bx^2 + cx + d \text{ with } x \in [0, L]. \quad (4)$$

This finite element is delimited by two nodes, each one characterised by a given pressure p and a pressure gradient $\partial p/\partial x$, for a total of four degrees of freedom. By substituting the definition of the degrees of freedom in the cubic polynomial, it is possible to derive the analytical expression of the four shape functions associated with the activation of each degree of freedom. These steps are omitted here for the sake of brevity. Finally, by imposing that the pressure field inside the duct must be a solution of the acoustic wave equation, the mass and stiffness matrix of each element were found:

$$[M] = \frac{A}{c^2}\begin{bmatrix} \frac{13}{35}L & \frac{11}{210}L^2 & \frac{9}{70}L & -\frac{13}{420}L^2 \\ \frac{11}{210}L^2 & \frac{1}{105}L^3 & \frac{13}{420}L^2 & -\frac{1}{140}L^3 \\ \frac{9}{70}L & \frac{13}{420}L^2 & \frac{13}{35}L & -\frac{11}{210}L^2 \\ -\frac{13}{420}L^2 & -\frac{1}{140}L^3 & -\frac{11}{210}L^2 & \frac{1}{105}L^3 \end{bmatrix} \quad (5)$$

$$[K] = A\begin{bmatrix} \frac{6}{5}L & \frac{1}{10} & -\frac{6}{5}L & \frac{1}{10} \\ \frac{1}{10} & \frac{2}{15}L & -\frac{1}{10} & -\frac{1}{30}L \\ -\frac{6}{5}L & -\frac{1}{10} & \frac{6}{5}L & -\frac{1}{10} \\ \frac{1}{10} & -\frac{1}{30}L & -\frac{1}{10} & \frac{2}{15}L \end{bmatrix} \quad (6)$$

This formulation was then implemented in a Matlab tool that models the tread grooves as a network of mono-dimensional finite elements. To define the model, the geometry of

each groove is reduced to its centreline and the cross-sectional area of each groove is stored in a dedicated table. The user also inputs whether specific grooves intersect with others. Then, the geometry is discretised to obtain a mesh of finite elements. At this point, the mass and the stiffness matrices of the whole network of grooves are evaluated, taking into account the connectivity of each element. Finally, boundary conditions are assigned at the grooves' terminations. In particular, if the user specifies an open-end condition, a null pressure is imposed at the outer node of the groove. On the other hand, in the case of a closed-end boundary condition, the nodal degree of freedom related to the pressure gradient is constrained.

This procedure was applied to the geometry investigated in the previous section. The resulting model is shown in Figure 11. In the representation, each finite element is coloured according to the imposed cross-sectional area. For this reason, all sipes are represented in green and lateral grooves in yellow, whereas circumferential grooves have different cross-sectional areas. The mesh nodes are represented using dots and, in the case of connected grooves, nodes are graphically connected using black lines. Open-end boundary conditions are represented as black triangles. At this stage, no end correction is applied, and this model is part of the Approach 3a class.

Once definition of the model was completed, the acoustic modes were found by solving the eigenvalue problem. These results were compared against the modes evaluated through Approach 1. As expected, the two sets of results were in accordance, both in terms of mode shapes and natural frequencies. For the sake of brevity, the mode shapes comparison is not shown, whereas the natural frequencies of the $(1, m)$ modes family

were already reported in Table 2. Looking at the results, Approach 3a seems to be slightly stiffer than Approach 1. However, the maximum mismatch among the results is approximately 50 Hz, which can be considered as a minor aspect, given the significant overestimation that both models show if compared with Approach 2.

To limit this overestimation of the natural frequencies, in Approach 3b an open-end boundary condition combined with end-corrections was implemented. The actual acoustic resonances are characterised by wavelengths that are longer than those estimated considering only the geometrical length of the circumferential grooves. For this reason, the end correction, being an additional fictitious acoustic length, may be added matching the real wavelengths to improve the results.

In general, end corrections are frequency-dependent and change according to the geometry near the duct end. For tyre noise applications, they are influenced by the curvature of the tyre surface near the grooves' terminations. In this work, to simplify their definition, two frequency-independent end corrections were derived, one for circumferential grooves and one for lateral grooves. This difference is justified by the different tyre curvature at the footprint inlet/outlet and regions. These end corrections were tuned using two detailed 3D models of a circumferential and a lateral groove carved in a 225/55R17 tyre loaded at 500 kg. For each model, the end correction ΔL was estimated from the resonance frequency f using the formula:

$$\Delta L = \frac{1}{2}\left(\frac{c}{2f} - L\right) \tag{7}$$

which derives from the expression of the resonance frequency of a duct with a length L with two open ends. The outcome of the tuning was a circumferential groove end-correction ΔL_c = 23 mm and a lateral one ΔL_l = 15 mm. These values agree with the range of possible end-corrections reported in [21].

Once the implementation of the end corrections was completed, the model shown in Figure 11 was upgraded. The resulting modes and natural frequencies are represented in Figure 12. As expected, the inclusion of end corrections caused the mode shapes to have a non-null pressure at the grooves' terminations, as the null pressure was imposed at an additional distance. Therefore, longer wavelengths were obtained, causing a significant reduction of the natural frequencies compared to the results of Approach 3a.

Considering that Approach 3b aims to provide results as close as possible to those of Approach 2, a comparison between these two methods was carried out. Firstly, looking at the mode shapes, it was concluded that the pressure fields estimated by the two approaches were in accordance. Secondly, a comparison in terms of natural frequencies was carried out (see Table 2). The inclusion of the end correction improved the match between the detailed model and the simplified ones, obtaining a satisfactory agreement for the $f_{1,2}$ and $f_{1,3}$ frequencies. However, overestimation of the $f_{1,1}$ frequency and underestimation of the $f_{1,4}$ were also present. This aspect is related to the definition of constant end corrections, as each mode would require a dedicated end correction to match the correct natural frequency. However, this solution was considered unfeasible,

as it would significantly increase the model's complexity and the tuning required, losing the benefits of using a simplified approach.

4. CONCLUSIONS

This work demonstrated the possibility of modelling the acoustic resonances of the tread grooves using the finite element technique, with increasing levels of complexity. Three modelling approaches were described, with differences in terms of modelled air volume, boundary conditions and procedures for defining the model's geometry.

These approaches agree in terms of estimated mode shapes. The analyses showed that, for the reference tread pattern, multiple pipe resonances are present due to the interaction between grooves, which generate modes with antinodes that can vibrate out-of-phase along the lateral and circumferential directions. To generalise, mode shapes of tread patterns with circumferential grooves can be classified according to a (n, m) nomenclature, where n and m are the number of antinodes along the two directions.

The modelling approaches show differences in terms of predicted natural frequencies. The results of the simplified Approach 1 and Approach 3a, even though in accordance with one another, showed a significant overestimation of the natural frequencies compared to Approach 2. This aspect is related to the unmodelled effect of the air that surrounds the footprint region, which causes wavelengths longer than the geometrical footprint dimensions. For this reason, to better approximate the real wavelengths, end corrections were implemented within Approach 3b.

411 The analyses showed that a detailed model based on Approach 2 and a simplified one
412 based on Approach 3b might be complementary tools for analysing acoustic resonances.
413 The first approach can model the phenomenon with fewer assumptions but requires a
414 more complex model setup and higher computational costs, limiting the possibility of
415 performing rapid assessments. On the other hand, simplified approaches might represent
416 an alternative for qualitative evaluations of the trends of acoustic resonances due to
417 geometrical modifications. For this reason, Approach 3b is recommended at the initial
418 stages of development of a new tread design, whereas detailed simulations based on
419 Approach 2 are recommended at the later stages.
420
421 To conclude, we wish to reiterate that the noise generated by a rolling tyre is the result
422 of the combined effect of generation and amplification mechanisms, which are both
423 influenced by the tread pattern geometry. For this reason, even though modelling of the
424 grooves' acoustic resonances is fundamental for analysing different design solutions,
425 studying generation mechanisms is relevant too. Therefore, if the simulation aim is to
426 predict the sound levels, models that integrate both mechanisms should be used.
427 Nonetheless, the investigation of each single aspect of the phenomenon is still relevant.
428 The analyses discussed in this paper are an investigation of a specific class of tread
429 patterns, however many other geometrical features could have been studied.
430 Nonetheless, the concepts described in this work are also applicable to the analysis of
431 other geometries. In addition, it is worth pointing out that, when it comes to designing a
432 tread pattern, several other performance factors must be guaranteed, such as dry and

433 wet handling, wear, hydroplaning, etc. Since the final design of a tread pattern is a
434 compromise between these requirements, simulations of these phenomena are
435 fundamental too, as they provide additional data and might help to reduce the number
436 of physical prototypes.
437

438 **ACKNOWLEDGMENT**

439 This study is part of the AirBorne tyre Exterior Noise (ABEN) project, carried out in the
440 framework of the Joint Labs cooperation agreement between Politecnico di Milano and
441 Pirelli. The authors gratefully acknowledge Pirelli for providing the support and data
442 necessary for this work.
443

444 **FUNDING**

445 This research did not receive any specific grant from funding agencies in the public,
446 commercial, or not-for-profit sectors.
447

448 **NOMENCLATURE**
449

A	Tread groove cross-sectional area
c	Sound speed
d	Tread groove equivalent diameter
f	Acoustic resonance frequency
f_{cut-on}	Cut-on frequency of cross-sectional modes
K	Stiffness matrix
L	Tread groove length
M	Mass matrix
p	Sound pressure
ΔL	End correction
φ	Acoustic mode shape
ω	Circular frequency $\omega = 2\pi f$

450
451

REFERENCES

[1] European Environment Agency, Environmental noise in Europe - 2020, Luxemburg, 2020.

[2] U. Sandberg, Tyre/road noise : myths and realities, in: 2001 International Congress and Exhibition on Noise Control Engineering, 2001.

[3] U. Sandberg, J.A. Ejsmont, Tyre/road Noise Reference Book, INFORMEX, 2002.

[4] U. Sandberg, J.A. Ejsmont, Tire/Road Noise—Generation, Measurement, and Abatement, in: Handbook of Noise and Vibration Control, John Wiley & Sons, Inc., Hoboken, NJ, USA, n.d.: pp. 1054–1071. https://doi.org/10.1002/9780470209707.ch86.

[5] X. Wang, Automotive Tire Noise and Vibrations, Elsevier, 2020. https://doi.org/10.1016/C2018-0-02431-7.

[6] G. Liao, M.S. Sakhaeifar, M. Heitzman, R. West, B. Waller, S. Wang, Y. Ding, The effects of pavement surface characteristics on tire/pavement noise, Applied Acoustics 76 (2014) 14–23. https://doi.org/10.1016/j.apacoust.2013.07.012.

[7] T. Li, R. Burdisso, C. Sandu, Literature review of models on tire-pavement interaction noise, J Sound Vib 420 (2018) 357–445. https://doi.org/10.1016/j.jsv.2018.01.026.

[8] J. Feng, C. Sandu, T. Li, R. Burdisso, The Effects of Tread Pattern on Tire Pavement Interaction Noise, in: INTER-NOISE 2016, 2016.

[9] J.A. Ejsmont, U. Sandberg, S. Taryma, Influence of Tread Pattern on Tire/Road Noise, SAE Transactions 93 (1984) 632–640.

[10] K. Larsson, S. Barrelet, W. Kropp, The modelling of the dynamic behaviour of tyre tread blocks, Applied Acoustics 63 (2002) 659–677. https://doi.org/10.1016/S0003-682X(01)00059-7.

[11] P. Gautam, A.J. Chandy, A Three-Dimensional Numerical Investigation of Air Pumping Noise Generation in Tires, J Vib Acoust 138 (2016). https://doi.org/10.1115/1.4034100.

[12] J. Eisenblaetter, S.J. Walsh, V. V. Krylov, Air-related mechanisms of noise generation by solid rubber tyres with cavities, Applied Acoustics 71 (2010) 854–860. https://doi.org/10.1016/j.apacoust.2010.05.002.

[13] R. Corradi, F. Ripamonti, R. Di Lione, M. Caccialanza, Test methodologies for mapping tyre exterior noise in semi-anechoic chamber, in: INTER-NOISE 2019, 2019.

[14] F. Kosaka, H. Fujii, Y. Kodama, A simulation and diagnosis of tire radiation noise, in: Internoise 2023 - 52nd International Congress and Exposition on Noise Control Engineering, 2023.

[15] T. Bravo, An analytical study on the amplification of the tyre rolling noise due to the horn effect, Applied Acoustics 123 (2017) 85–92. https://doi.org/10.1016/j.apacoust.2017.03.009.

[16] R.A.G. GRAF, C.-Y. KUO, A.P. DOWLING, W.R. GRAHAM, ON THE HORN EFFECT OF A TYRE/ROAD INTERFACE, PART I: EXPERIMENT AND COMPUTATION, J Sound Vib 256 (2002) 417–431. https://doi.org/10.1006/jsvi.2001.4238.

[17] C.-Y. KUO, R.A.G. GRAF, A.P. DOWLING, W.R. GRAHAM, ON THE HORN EFFECT OF A TYRE/ROAD INTERFACE, PART II: ASYMPTOTIC THEORIES, J Sound Vib 256 (2002) 433–445. https://doi.org/10.1006/jsvi.2001.4217.

[18] A.D. Pierce, Acoustics: An Introduction to Its Physical Principles and Applications, Springer International Publishing, Cham, 2019. https://doi.org/10.1007/978-3-030-11214-1.

[19] J.-P. DALMONT, C.J. NEDERVEEN, N. JOLY, RADIATION IMPEDANCE OF TUBES WITH DIFFERENT FLANGES: NUMERICAL AND EXPERIMENTAL INVESTIGATIONS, J Sound Vib 244 (2001) 505–534. https://doi.org/10.1006/jsvi.2000.3487.

[20] S. Mohammadi, A. Ohadi, A novel approach to design quiet tires, based on multi-objective minimization of generated noise, Applied Acoustics 175 (2021) 107825. https://doi.org/10.1016/j.apacoust.2020.107825.

[21] Y. Saito, Mechanism of tire / road noise emission and reduction technology, in: Internoise 2023 - 52nd International Congress and Exposition on Noise Control Engineering, 2023.

[22] B. Wang, D. Duhamel, On the design and optimization of acoustic network resonators for tire/road noise reduction, Applied Acoustics 120 (2017) 75–84. https://doi.org/10.1016/j.apacoust.2017.01.017.

[23] D. Duhamel, B. Wang, Horn effect of tyre/road noise: modelling and experiments of acoustic network resonators in horn-like structures, International Journal of Vehicle Noise and Vibration 14 (2018) 191. https://doi.org/10.1504/IJVNV.2018.10016439.

[24] J. Pinay, Y. Saito, C. Mignot, F. Gauterin, Understanding the contribution of groove resonance to tire-road noise on different surfaces under various operating conditions, Acta Acustica 4 (2020) 6. https://doi.org/10.1051/aacus/2020004.

[25] W. Kropp, F.-X. Bécot, S. Barrelet, On the Sound Radiation from Tyres, Acta Acustica United with Acustica 86 (2000) 769–779.

[26] Fahy, F., & Walker, J., Advanced Applications in Acoustics, Noise and Vibration (1st ed.), CRC Press (2004), https://doi.org/10.1201/9781315273396

545 **Figure Captions List**
546

Fig. 1 The geometrical model of a circumferential groove is shown on the left. The first and the second acoustic resonances are represented on the right.

Fig. 2 Inclusion of the lateral grooves with open ends and their effect on the acoustic mode shapes and natural frequencies.

Fig. 3 Effect of lateral grooves with closed ends (represented as black terminations) on the mode shapes and natural frequencies.

Fig. 4 Effect of the lateral grooves' length on the resonance frequencies. On the left, the effect of open-end lateral grooves; on the right, closed-end grooves. Each marker represents a simulation result.

Fig. 5 Effect of the number of lateral grooves on the resonance frequencies, considering open-end or closed-end lateral grooves.

Fig. 6 Effect on the resonances of different positions of the lateral grooves, considering a progressive shift of fractions of a pitch dimension (25 mm for this model).

Fig. 7 Model for investigating the acoustic resonances of a tread pattern based on Approach 1.

Fig. 8 Modes with lowest frequencies, computed using Approach 1. These results are all part of the mode family $(1, m)$. A detail of the pressure variation inside a sipe is shown for the last resonance.

Fig. 9 The acoustic model based on Approach 2. The geometry of the deformed treaded tyre in contact with the drum is represented on the left. A detail of the footprint region is shown on the right.

Fig. 10 Mode shapes and natural frequencies of the mode family $(1, m)$ evaluated using Approach 2.

Fig. 11 In Approaches 3a and 3b, the footprint geometry is schematised as a network of mono-dimensional finite elements. Different colours are used to represent different cross-sectional areas.

Fig. 12 Mode shapes and natural frequencies evaluated using Approach 3b.

547
548

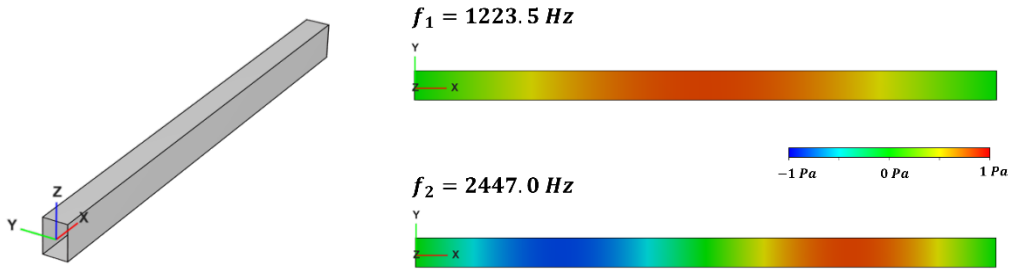

549

550 Figure 1 The geometrical model of a circumferential groove is shown on the left. The first

551 and the second acoustic resonances are represented on the right.

552

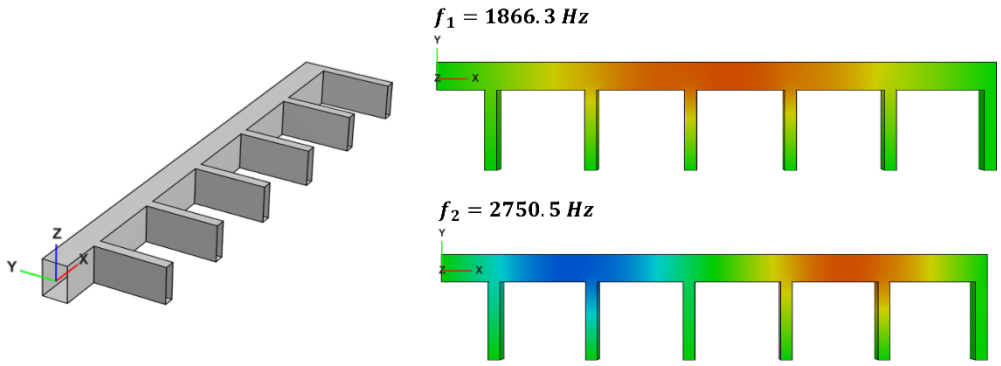

Figure 2 Inclusion of the lateral grooves with open ends and their effect on the acoustic mode shapes and natural frequencies.

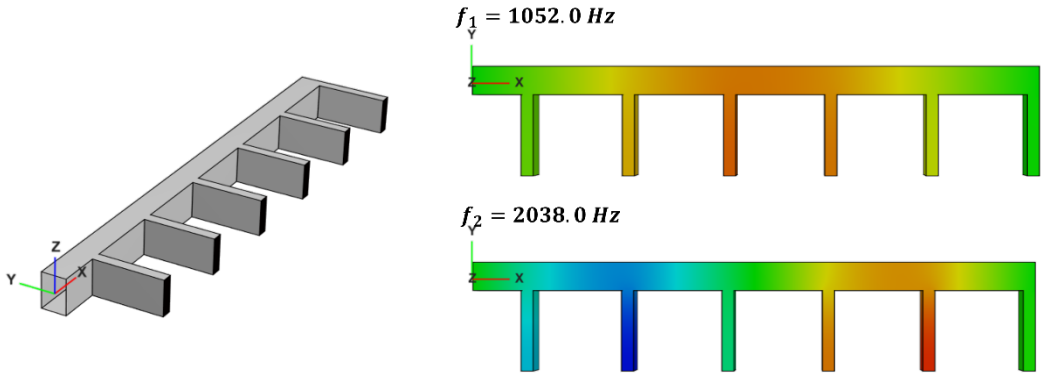

Figure 3 Effect of lateral grooves with closed ends (represented as black terminations) on the mode shapes and natural frequencies.

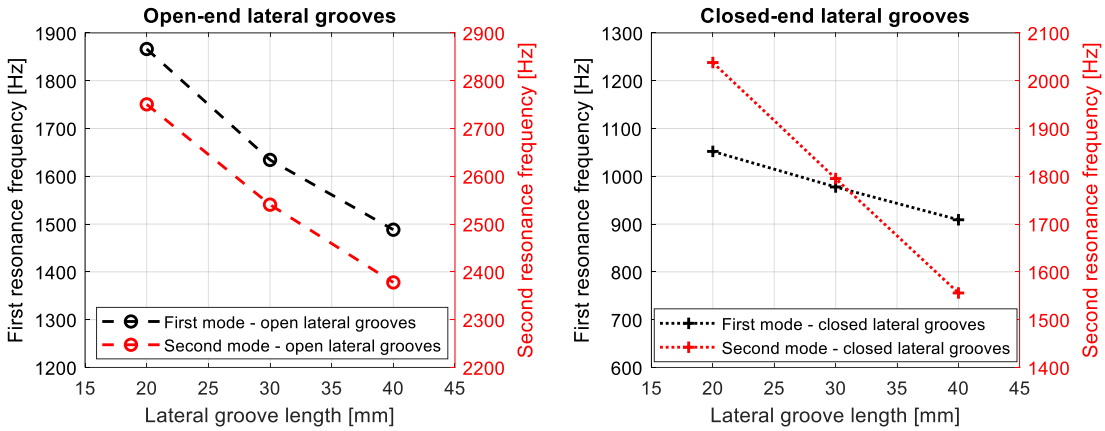

Figure 4 Effect of the lateral grooves' length on the resonance frequencies. On the left, the effect of open-end lateral grooves; on the right, closed-end grooves. Each marker represents a simulation result.

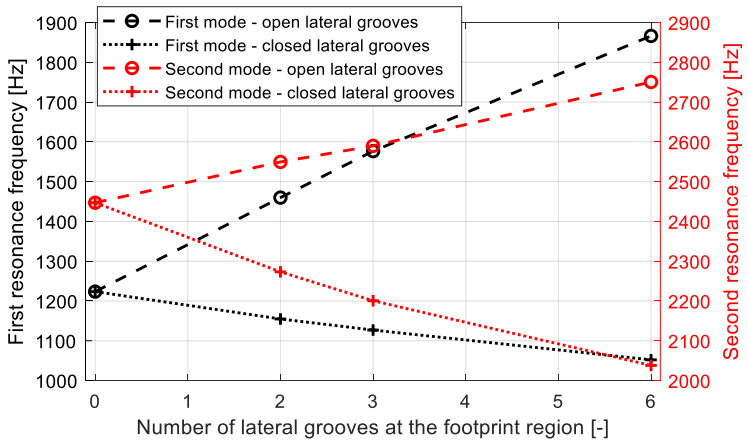

Figure 5 Effect of the number of lateral grooves on the resonance frequencies, considering open-end or closed-end lateral grooves.

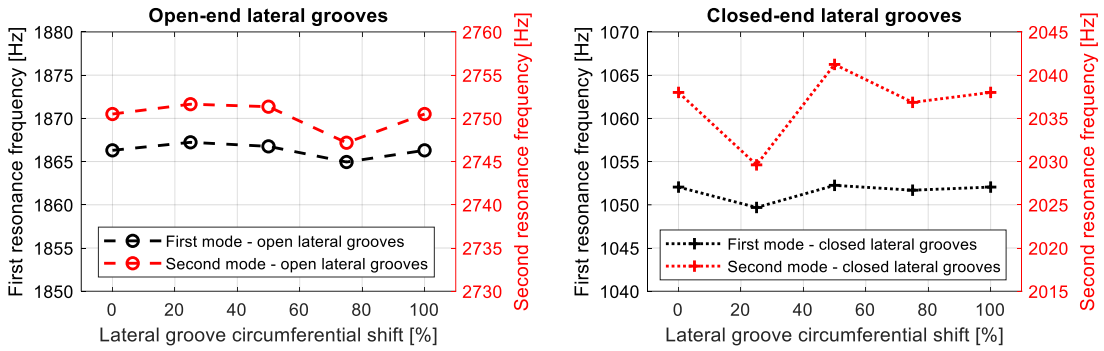

570

571 Figure 6 Effect on the resonances of different positions of the lateral grooves, considering

572 a progressive shift of fractions of a pitch dimension (25 mm for this model).

573

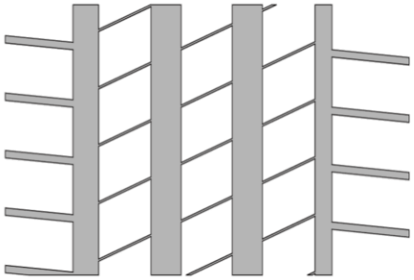

Figure 7 Model for investigating the acoustic resonances of a tread pattern based on Approach 1.

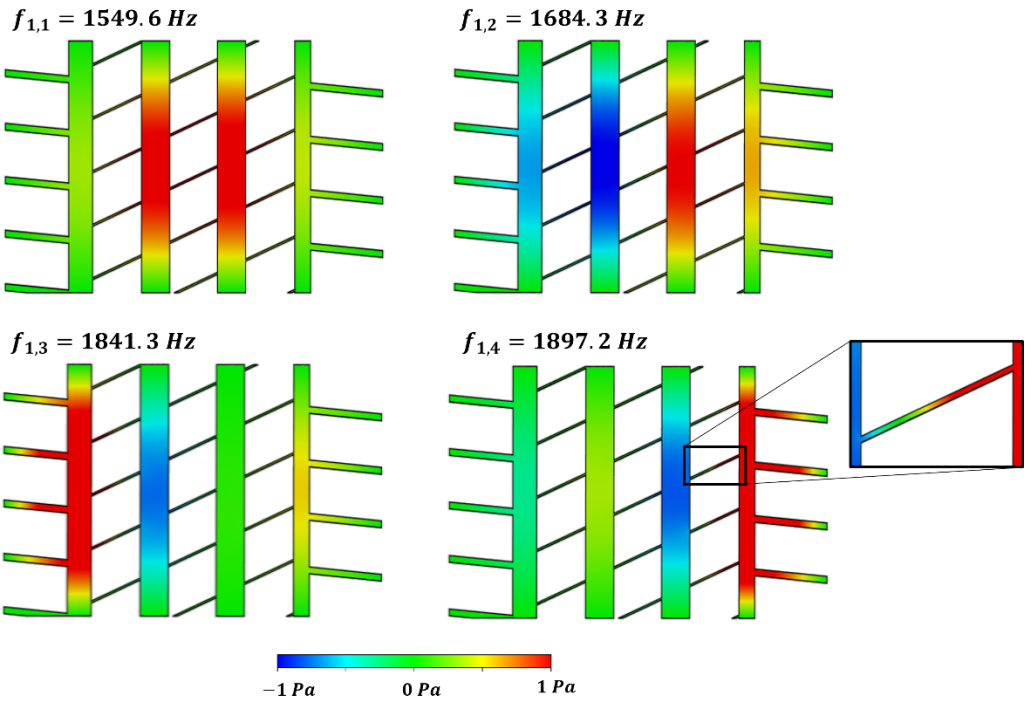

Figure 8 Modes with lowest frequencies, computed using Approach 1. These results are all part of the mode family $(1, m)$. A detail of the pressure variation inside a sipe is shown for the last resonance.

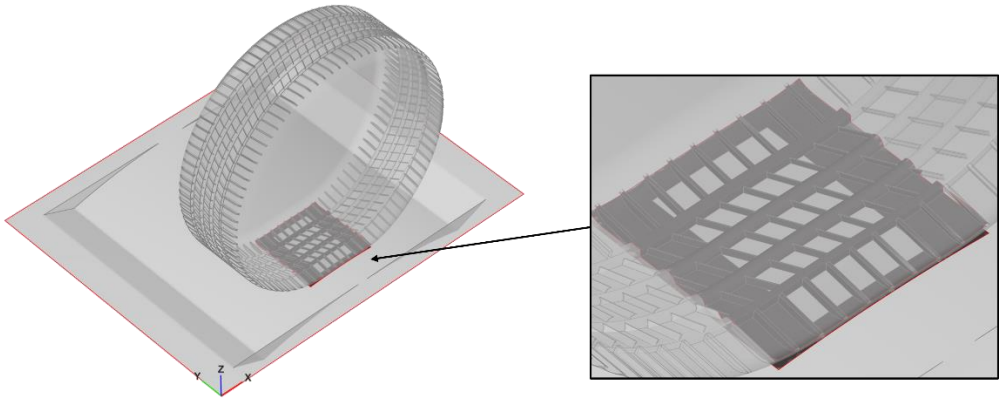

Figure 9 The acoustic model based on Approach 2. The geometry of the deformed treaded tyre in contact with the drum is represented on the left. A detail of the footprint region is shown on the right.

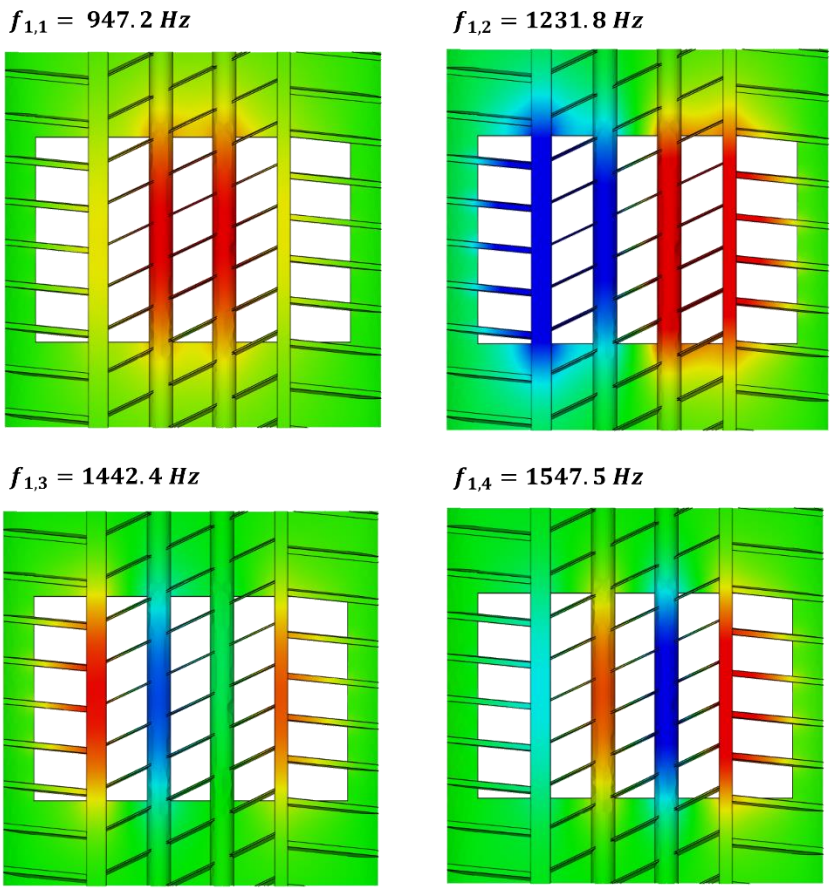

Figure 10 Mode shapes and natural frequencies of the mode family $(1, m)$ evaluated using Approach 2.

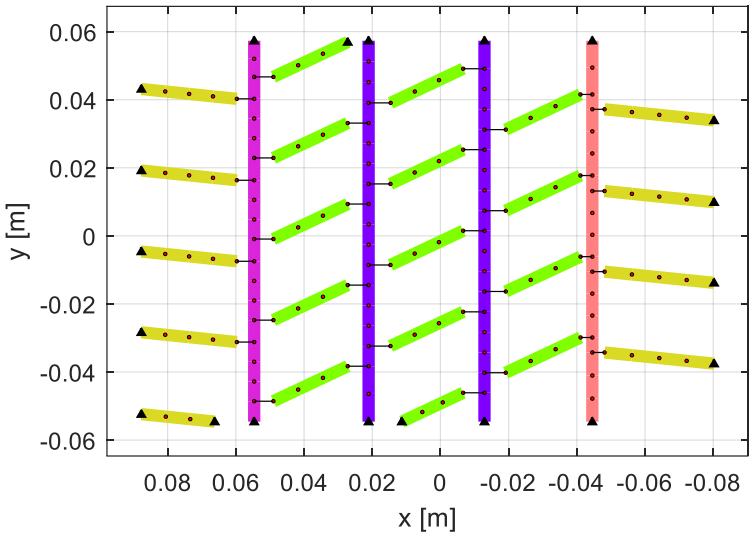

Figure 11 In Approaches 3a and 3b, the footprint geometry is schematised as a network of mono-dimensional finite elements. Different colours are used to represent different cross-sectional areas.

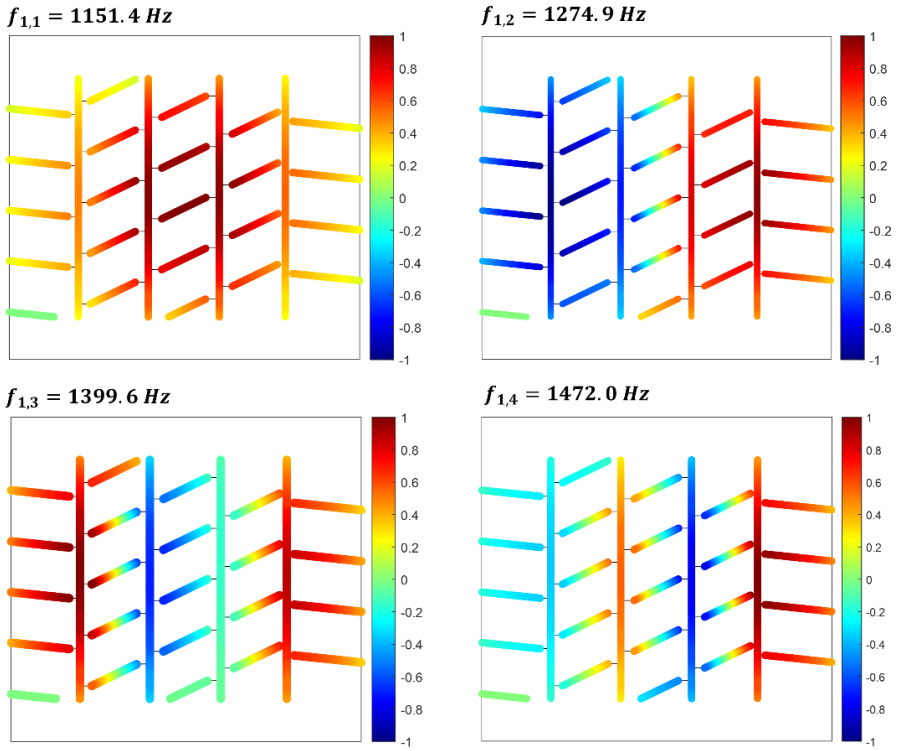

595

596 Figure 12 Mode shapes and natural frequencies evaluated using Approach 3b.

597

598 **Table Caption List**
599

Table 1 Definition of the modelling approaches discussed in this paper.

Table 2 Comparison of natural frequencies evaluated using the modelling approach discussed in this paper.

600
601

602 Table 1 Definition of the modelling approaches discussed in this paper.

Approach	**Features**		
	Modelled air volume	**Geometry definition**	**End correction**
Approach 1	Only the air inside the tread grooves at the footprint region	Based on 3D geometries developed in CAD environment	Not applied
Approach 2	Air surrounding the whole tyre and including all grooves	Based on a 3D deformed tyre simulation (finite element structural analysis)	Not required
Approach 3a	Only the air inside the tread grooves at the footprint region	Based on a network of grooves' centrelines with a given cross-sectional area	Not applied
Approach 3b	As Approach 3a	As Approach 3a	Applied

603
604

605 Table 2 Comparison of natural frequencies evaluated using the modelling approach
606 discussed in this paper.

	$f_{1,1}$	$f_{1,2}$	$f_{1,3}$	$f_{1,4}$
Approach 1	1549.6 Hz	1684.3 Hz	1841.3 Hz	1897.2 Hz
Approach 2	947.2 Hz	1231.8 Hz	1442.4 Hz	1547.5 Hz
Approach 3a	1594.3 Hz	1729.3 Hz	1891.9 Hz	1921.1 Hz
Approach 3b	1151.4 Hz	1274.9 Hz	1399.6 Hz	1472.0 Hz

607